Progress In Electromagnetics Research, PIER 23, 187–219, 1999

ACCURATE ANALYSIS OF A CYLINDRICAL DIELECTRIC RESONATOR MOUNTED ON A GROUNDED DIELECTRIC SUBSTRATE

G. J. Karonis, D. I. Kaklamani, and N. K. Uzunoglu

Department of Electrical and Computer Engineering
National Technical University of Athens
9 Iroon Polytechnious Street
GR-15780 Zografos, Athens, Greece

1. Introduction
2. Formulation of the Resonance Problem
3. Solution of the Integral Equation
4. Computation of the "Impedance Terms" and "Source Terms"
5. Numerical Results
6. Conclusions
Appendices
References

1. INTRODUCTION

Dielectric resonators have become important components of microwave systems in designing filters, oscillators, amplifiers and tuners [1]. This is mainly due to their high-Q (low-loss) value and their contribution to miniaturization of microwave circuits. The resonance properties of dielectric cylinders have been studied in the past using various approaches based on the Perfectly Magnetic Conductor (PMC) wall assumption [2], the Dielectric Waveguide Model (DWM) [3] and its improvements [4], the Effective Dielectric Constant (EDC) method [5], Mode Matching (MM) methods [6–10], Integral Equation (IE) and Method of Moments (MoM) techniques [11–15], Generalized Impedance Boundary Condition (GIBC) methods [16], Finite Elements

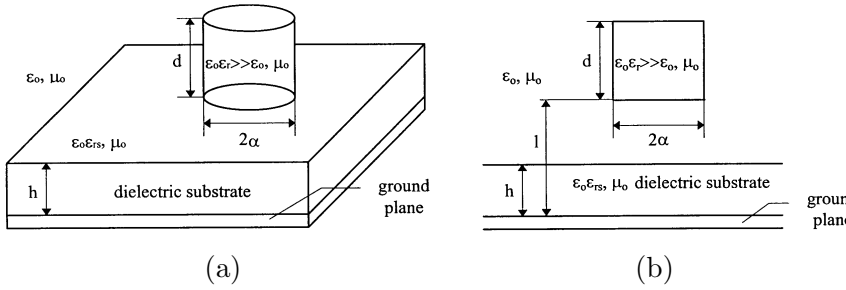

Figure 1. Dielectric cylindrical geometry.

(FE) methods [17], Finite Difference Frequency Domain (FDFD) methods [18, 19] and Finite Difference Time Domain (FDTD) methods [20, 21], assuming non-radiating structures. Usually, the dielectric resonator is of finite height cylindrical shape with a very large dielectric permittivity ($\varepsilon_r \approx 30$) and, in many cases, the resonance properties are treated considering the dielectric cylindrical resonator isolated in space [8, 9, 12, 20–28]. Nevertheless, the resonance properties of dielectric cylinders is highly dependent on the electromagnetic (EM) properties of the neighbouring object, the most common case being the grounded dielectric substrate used in microstrip technology circuits. Indeed, the extensive use of microstrip technology, compatible to high permittivity finite cylinder dielectric resonators, requires the development of accurate computational techniques to determine their resonance properties and especially the effects of EM structures being in their vicinity. This is due to the fact that, the very high value of the cylinders' dielectric permittivity seems to cause numerical instability and serious convergence problems on the computational techniques to be used, which are otherwise very stable and easily convergent for low dielectric permittivity values. Considering the necessity of computing the resonance frequency with an accuracy better than 50 ppm, very accurate and highly convergent methods need to be developed, such as IE-MoM techniques used in previous works [14, 15]. Especially for "open" structures, as in the present case, MoM/Galerkin techniques with a "proper" set of basis functions seem to be more promising in terms of accuracy compared to FDTD and FE based methods.

To this end, in the present paper, an open dielectric resonator is analyzed, using a volume integral equation formulation in conjunction with a Galerkin technique to determine the resonance frequencies, as

well as the quality factors (Q). The geometry of the resonator structure is shown in Figure 1(a). A cylinder of height d and radius a with a high permittivity value $(\varepsilon_r \gg 1)$ is placed above a grounded dielectric substrate of permittivity ers and height h. For the sake of generality, the pursued analysis is also valid for the case where there is an $(1-h)$ distance between the resonator and the grounded dielectric substrate, as shown in Figure 1(b). The geometry presented in Figure 1(a) corresponds to the case $1 = h$, while for $1 \to \propto$ the resonator is isolated in the free space. In the following, the excitation structure is considered to be a Hertzian dipole instead of a microstrip line. The time dependence of the EM oscillation is assumed to be $\exp(-i\omega t)$ and is suppressed throughout the analysis.

In section 2, the formulation of the problem is presented and an integral equation is derived in terms of the electric field inside the resonator, which is solved in section 3, via an entire domain Galerkin technique. The specific computations needed to calculate the kernel and the right hand side elements are given in section 4. Numerical results are presented in section 5 for several resonator sizes and operation frequencies and the resonance properties of the examined structure are determined, while concluding remarks and topics for further work are given in section 6.

2. FORMULATION OF THE RESONANCE PROBLEM

In order to determine the resonance properties of the structure shown in Figure 1, the dyadic Green's function $\overline{\underline{G}}(\underline{r}, \underline{r}')$ of the grounded substrate has to be taken into consideration. To this end, the expression derived in [29] for a Hertzian dipole excitation parallel to the microstrip substrate is extended and generalized, assuming an arbitrarily oriented elementary dipole as a primary source, with a current density $\underline{J}(\underline{r}) = p_o\hat{\delta}\delta(\underline{r} - \underline{r}_o)$, where $p_o(A \cdot m)$ is the electric dipole moment, $\hat{\delta}$ is the unit vector defining the dipole orientation and $\delta(\underline{r} - \underline{r}_o)$ is the three-dimensional (3D) Dirac delta function, with $\underline{r}_o$ denoting the dipole position.

Since the entire space is magnetically homogeneous, applying the Green's theorem, the fundamental equation is obtained, as [30]

$$\underline{E}(\underline{r}) = k_o^2(\varepsilon_r - 1) \iiint\limits_{V_d} d\underline{r}' \; \overline{\underline{G}}(\underline{r}, \underline{r}') \cdot \underline{E}(\underline{r}') + p_o\hat{\delta} \cdot \overline{\underline{G}}(\underline{r}, \underline{r}_o) \qquad (1)$$

where V_d is the finite height dielectric cylinder volume and $\underline{E}(\underline{r})$ is the unknown electric field distribution inside the cylindrical dielectric resonator. The physical interpretation of eq. (1), when $\underline{r}$ is kept within the dielectric resonator volume V_d, is the regeneration of the electric field itself, due to the reaction of the dielectric cylinder in the presence of the grounded substrate. Restricting the observation point $\underline{r}$ within V_d, eq. (1) forms a 3D integral equation in terms of $\underline{E}(\underline{r})$, which is solved, as presented in section 3, applying a Galerkin procedure.

3. SOLUTION OF THE INTEGRAL EQUATION

Since the unknown electric field quantity $\underline{E}(\underline{r})$ inside the dielectric resonator volume V_d, represents a finite energy vector function, it can be expanded into a Fourier integral, as

$$\underline{E}(\underline{r}) = \int_{-\infty}^{+\infty}\int\int d\underline{k}\, \exp(i\underline{k}\cdot\underline{r})\underline{C}(\underline{k}) \tag{2}$$

where each individual $\{\exp(i\underline{k}\cdot\underline{r})\underline{C}(\underline{k})\}$ wave term should satisfy the appropriate wave equation

$$\nabla\times\nabla\times\underline{E}(\underline{r}) - k_o^2\varepsilon_r\underline{E}(\underline{r}) = 0 \tag{3}$$

This shows that, for an isotropic dielectric, as in the present case, it is $|\underline{k}| = k_d = k_o\sqrt{\varepsilon_r}$ and the 3D integral in eq. (2) should be restricted only to the two angular variables, namely the θ_k and ϕ_k angles in the phase space, as

$$\underline{E}(\underline{r}) = \iint_{\Omega_k} d\hat{k}\ \underline{C}(\hat{k})\exp(ik_d\hat{k}\cdot\underline{r}) \equiv \int_0^{2\pi} d\phi_k \int_0^{\pi} d\theta_k\ \sin\theta_k\underline{C}(\hat{k})\exp(ik_d\hat{k}\cdot\underline{r}) \tag{4}$$

where $\underline{r}\in V_d$, $k_d = k_o\sqrt{\varepsilon_r}$ is the wavenumber in the dielectric resonator region, $\hat{k} = \hat{z}\cos\theta_k + (\hat{x}\cos\phi_k + \hat{y}\sin\phi_k)\sin\theta_k$ is an arbitrary unit vector in the spectral space Ω_k and $\underline{C}(\hat{k})$ is the 3D unknown spectral function.

On substituting eq. (4) into eq. (1), calculating the moment over the volume V_d and using as test functions the same set of

$\exp(-ik_d\hat{\xi}\cdot\underline{r})$ functions (Galerkin technique), the following integral equation is obtained

$$\iint\limits_{\Omega_k} d\hat{k}\ \overline{\underline{K}}(\hat{\xi},\hat{k})\cdot\underline{C}(\hat{k}) = \underline{B}(\hat{\xi}) \tag{5}$$

where the kernel

$$\begin{aligned}\overline{\underline{K}}(\hat{\xi},\hat{k}) = &\iiint\limits_{V_d} d\underline{r}\exp[-ik_d(\hat{\xi}-\hat{k})\cdot\underline{r}] \\ &- k_o^2(\varepsilon_r-1)\iiint\limits_{V_d} d\underline{r}\iiint\limits_{V_d} d\underline{r}'\ \exp(-ik_d\hat{\xi}\cdot\underline{r})\cdot\overline{\underline{G}}(\underline{r},\underline{r}')\cdot\exp(ik_d\hat{k}\cdot\underline{r}')\end{aligned} \tag{6}$$

is referred to as "Impedance Matrix" and the right hand term

$$\underline{B}(\hat{\xi}) = \iiint\limits_{V_d} d\underline{r}\ \exp[-ik_d\hat{\xi}\cdot\underline{r}]\ \overline{\underline{G}}(\underline{r},\underline{r}_o)\cdot\hat{\delta}p_o \tag{7}$$

denotes the primary source impact. The techniques employed to compute the $\overline{\underline{K}}(\hat{\xi},\hat{k})$ and $\underline{B}(\hat{\xi})$ elements are described in section 4.

In order to solve eq. (5), considering the non-singular character of the kernel $\overline{\underline{K}}(\hat{\xi},\hat{k})$, a discretization procedure is implemented to convert this equation to a linear system with finite number of unknowns. To this end, the Fourier transformation given by eq. (4) is converted into a discrete summation with distributed values, as

$$\underline{E}(\underline{r}) = \sum_{k=1}^{K}\sum_{l=1}^{L}\underline{C}(\hat{k}_{kl})\exp\left[ik_d(\hat{k}_{kl}\cdot\underline{r})\right] \tag{8}$$

where $\underline{C}(\hat{k}_{kl}) = \underline{C}(k,l) = C_{kl}^x\hat{x} + C_{kl}^y\hat{y} + C_{kl}^z\hat{z}$ is a new unknown coefficient in which the terms $\sin(k\Delta\theta)$ and the weighting coefficients derived from the discretization procedure are incorporated, the "pivot" vectors are

$$\hat{k}_{kl} = \sin(k\Delta\theta)[\cos(l\Delta\varphi)\hat{x} + \sin(l\Delta\varphi)\hat{y}] + \cos(k\Delta\theta)\hat{z}) \tag{9}$$

and the correspondences

$$\theta_k \leftrightarrow k\Delta\theta \quad \text{and} \quad \phi_k \leftrightarrow l\Delta\phi \quad \text{with} \quad \Delta\theta = \frac{\pi}{K+1} \quad \text{and} \quad \Delta\phi = \frac{2\pi}{L} \tag{10}$$

are valid. Therefore, eq. (5) is converted to the 3KL order linear system

$$\sum_{k=1}^{K} \sum_{l=1}^{L} \overline{\underline{K}}(\hat{\xi}_{k'l'}, \hat{k}_{kl}) \cdot \underline{C}(\hat{k}_{kl}) = \underline{B}(\hat{\xi}_{k'l'}) \tag{11}$$

where eqs. (9)–(10) are also valid for the set of $\{\hat{\xi}_{k'l'} \ |k' = 1, 2, \ldots K/1' = 1, 2, \cdots, L\}$ "testing" pivots and the "impedance matrix" elements $\overline{\underline{K}}(\hat{\xi}_{k'l'}, \hat{k}_{kl})$ and the "source term" elements $\underline{B}(\hat{\xi}_{k'l'})$ are defined in the next section 4. The number of K and L pivot-vectors is selected based on convergence considerations, discussed in section 5 and, finally, eq. (11) is numerically inverted, using a Gauss triangulation technique. Note that, as already proved in previous works [31], the convergence of the proposed Galerkin technique accelerates due to the fact that, each individual basis function is chosen to satisfy the corresponding wave equation (3) inside the cylindrical dielectric resonator.

4. COMPUTATION OF THE "IMPEDANCE TERMS" AND "SOURCE TERMS"

In order to compute the "impedance matrix" elements $\overline{\underline{K}}(\hat{\xi}_{k'l'}, \hat{k}_{kl})$ and the "source term" elements $\underline{B}(\hat{\xi}_{k'l'})$ appearing in eq. (11), the Fourier expansion of the scalar Green's function is employed, as

$$\frac{\exp(ik_0|\underline{r} - \underline{r}'|)}{4\pi|\underline{r} - \underline{r}'|} = \frac{1}{(2\pi)^3} \lim_{\varepsilon \to 0^+} \int_{-\infty}^{+\infty} dp_x \int_{-\infty}^{+\infty} dp_y \int_{-\infty}^{+\infty} dpz \, \frac{\exp(i\underline{p} \cdot (\underline{r} - \underline{r}'))}{p^2 - k_0^2 - i\varepsilon} \tag{12}$$

where $\underline{p} = (p_x, p_y, p_z)$ and $p^2 = p_x^2 + p_y^2 + p_z^2$. Then, expressing the dyadic Green's function $\overline{\underline{G}}(\underline{r}, \underline{r}')$ as a superposition of the free-space Green's function $\overline{\underline{G}}_o(\underline{r}, \underline{r}')$ and the dyadic $\overline{\underline{G}}_1(\underline{r}, \underline{r}')$, associated to the microstrip substrate, the following representation is derived

$$\begin{aligned}\overline{\underline{G}}(\underline{r},\underline{r}') &= \overline{\underline{G}}_o(\underline{r},\underline{r}') + \overline{\underline{G}}_1(\underline{r},\underline{r}') \\ &= \frac{1}{8\pi^3}\int\limits_{\substack{-\infty\\ \varepsilon\to 0^+}}^{+\infty}\int d\underline{p}\ \frac{(p^2\overline{\underline{I}} - \underline{pp})}{p^2 - k_0^2 - i\varepsilon}\ e^{i\underline{p}\cdot(\underline{r}-\underline{r}')} + \\ &\quad + \frac{1}{8\pi^2}\iint\limits_{-\infty}^{+\infty} dp_x dp_y\ \overline{\underline{g}}_1(p_x,p_y) e^{ip_x(x-x')+ip_y(y-y')-\mu(z+z'-2h)}\end{aligned} \tag{13}$$

where $\overline{\underline{g}}_1$ is given in Appendix I and

$$\mu = \sqrt{p_x^2 + p_y^2 - k_0^2} \quad \text{with} \quad \text{Real}(\mu) > 0 \quad \text{and} \quad \text{Imag}(\mu) < 0 \tag{14}$$

in accordance to the $\exp(-i\omega t)$ time dependence and the satisfaction of the radiation condition at infinity.

After substituting eq. (13) into eq. (11), the integrations with respect to the (x, y, z) and (x', y', z') variable s are of the type

$$U_1 = \int\limits_{V_d} d\underline{r}\ e^{i\underline{\beta}\cdot\underline{r}} = \int\limits_0^{\alpha} d\rho \int\limits_0^{2\pi} \rho d\phi \int\limits_l^{l+d} dz\ \exp\{i(\rho_\beta \rho\cos(\phi_\beta - \phi) + \beta_z z)\} \tag{15}$$

with $\underline{\beta} = \rho_\beta\hat{\rho} + \phi_\beta\hat{\phi} + \beta_z\hat{z}$ and are carried out analytically, as

$$U_1(\beta) = 2\pi\alpha^2\ \frac{J_1(\rho_\beta\alpha)}{\rho_\beta\alpha} \cdot \frac{2\sin\left(\beta_z\dfrac{d}{2}\right)}{\beta_z}\ e^{i\beta_z\left(1+\frac{d}{2}\right)} \tag{16}$$

making use of the formula 9.1.18 of [32]

$$2\pi J_0(\tau) = \int\limits_0^{2\pi} d\phi\ e^{i\tau\cos\phi} \tag{17}$$

Then, all the derived integrals with respect to the p_z term, appearing in the $\overline{\underline{G}}_o(\underline{r},\underline{r}')$ term of eq. (13), are of the type

$$\lim_{\varepsilon\to 0^+} \int\limits_{-\infty}^{+\infty} dp_z\ \frac{f(p_z)}{p^2 - k_0^2 - i\varepsilon}\ \exp(i\alpha p_z)\ \ , \quad \alpha \neq 0 \tag{18}$$

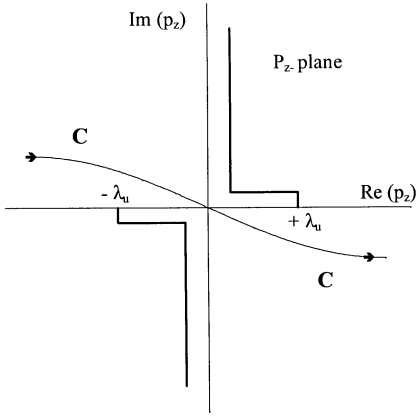

Figure 2. Complex plane geometry.

having poles at the points $\pm\lambda_u$ with $\lambda_u^2 = k_0^2 - p_x^2 - p_y^2 + i\varepsilon,\ \varepsilon \to 0^+$ and, therefore, their values are also carried out analytically, using contour integration methods (Cauchy theorem). In each case, the contour C shown in Figure 2 is closed depending on the number α sign.

After having carried out analytically the integrations with respect to the (x, y, z), (x', y', z') and p_z variables, as described above, two dimensional integrals in the spectral space (p_x, p_y) are obtained, which are numerically computed, based on a Gauss quadrature integration method presented in p. 887 and p. 916 of [32]. Sufficient accuracy is then achieved, by increasing both the number of integration points and the integrals' bounds truncation. To this end, the double integrals with respect to the variables p_x and p_y are transformed in cylindrical coordinates as

$$\int_{-\infty}^{+\infty} dp_x \int_{-\infty}^{+\infty} dp_y \equiv \int_{0}^{+\infty} d\rho_p\ \rho_p \int_{0}^{2\pi} d\phi_p \quad , \quad p_x = \rho_p \cos\phi_p,\ p_y = \rho_p \sin\phi_p \tag{19}$$

so that the convergence only with respect to the ρ_p integration upper limit has to be checked.

Following the above described procedure, the "impedance matrix" elements $\underline{\overline{K}}(\hat{\xi}_{k'l'}, \hat{k}_{kl})$ and the "source term" elements $\underline{B}(\hat{\xi}_{k'l'})$ are defined in Appendix II.

5. NUMERICAL RESULTS

If the examined resonator problem is faced as a homogeneous problem, then in eq. (11) it would be $\underline{B}(\hat{\xi}_{k'l'}) = 0$ and the resonance frequencies could be determined by computing the complex roots of the corresponding kernel determinant $\det[\,\overline{\underline{K}}(\hat{\xi}_{k'l'}, \hat{k}_{kl})]$ for the $\dot{k}_0 = \dot{\omega}/c$ variable, where $\dot{k}_0$ and $\dot{w}$ is the complex wavenumber and the complex frequency, respectively. However, this task has been proved to lead to numerical difficulties [33], due to the involvement of the two variables $\mathrm{Real}(k_0)$ and $\mathrm{Imag}(k_0)$. To this end, in the present work, an alternative method, based on the assumption of an external source is applied, leading to a numerically stable solution.

Namely, in order to determine the resonance properties, the stored average electric field energy is computed, based on the expression

$$P_\varepsilon = \frac{\varepsilon_o \varepsilon_r}{4} \iiint\limits_{V_d} d\underline{r}\ \underline{E}(\underline{r}) \cdot \underline{E}^*(\underline{r}) \tag{20}$$

and substituting eq. (2) into eq. (20), after some simple algebra, it is shown that

$$\begin{aligned} P_\varepsilon &= \frac{\varepsilon_o \varepsilon_r}{4} \iint\limits_{\Omega_k} d\hat{k} \iint\limits_{\Omega_k} d\hat{\xi}\ \underline{C}(\hat{k}) \cdot \underline{C}^*(\hat{\xi}) U(\hat{k} - \hat{\xi}) \Rightarrow \\ P_\varepsilon &= \frac{\varepsilon_o \varepsilon_r}{4} \sum_{k=1}^{K} \sum_{l=1}^{L} \sum_{k'=1}^{K} \sum_{l'=1}^{L} \underline{C}(\hat{k}_{kl}) \cdot \underline{C}^*(\hat{\xi}_{k'l'}) U(\hat{k}_{kl} - \hat{\xi}_{k'l'}) \end{aligned} \tag{21}$$

where exactly the same discretization procedure as in eqs (8)–(11) is employed, with $U(\hat{k}_{kl} - \hat{\xi}_{k'l'}) = \iiint\limits_{V_d} d\underline{r}\ \exp[+ik_d(\hat{k}_{kl} - \hat{\xi}_{k'l'}) \cdot \underline{r}]$ being calculated as described in eqs (15)–(17).

In order to determine the resonant frequencies "f_n" and the corresponding quality factors "Q_n", a frequency scanning technique is employed, by varying the oscillation frequency f of the primary current source. An approximate estimation of the resonant frequency for the dominant mode $(\mathrm{TE}_{01\delta})$ of an isolated dielectric resonator can be found by using the formula (see p. 3 of [1])

$$f_{approx} = \frac{34}{\alpha\sqrt{\varepsilon_r}} \left(\frac{\alpha}{d} + 3.45 \right) \tag{22}$$

where α, d denote the cylinder radius and height respectively and are expressed in mm, while f_{approx} is expressed in GHz. Then, eq. (11) is solved consequently for various frequencies f in the region of f_{approx} and the stored electric energy P_ε is computed as a function of frequency. A resonance behaviour is observed, independently of the primary excitation, presenting peak values with narrow linewidth.

In order to insure convergence, in the first place, accurate computation of the $\overline{\underline{K}}(\hat{\xi}_n, \hat{k}_n)$ and $\underline{B}(\hat{\xi}_n)$ terms (see eq. (11)) is required, which—according to the formulae given in Appendix II—corresponds to accurate computation of $\int_0^{+\infty} d\rho_p \; \rho_p \int_0^{2\pi} d\phi_p \; f(\rho_p, \phi_p)$ integrals. Sufficient accuracy is achieved, by increasing both the number of integration points and the ρ_p integration upper bound truncation. For the $\overline{\underline{K}}(\hat{\xi}_n, \hat{k}_n)$ elements, in the worst case, the integrand $f(\rho_p, \phi_p)_{\rho_p \longrightarrow \infty} \frac{1}{\rho_p^3}$, while for the $\underline{B}(\hat{\xi}_n)$, in the worst case, the integrand $f(\rho_p, \phi_p)_{\rho_p \longrightarrow \infty} \frac{1}{\rho_p^2}$, and the ρ_p integration upper limit is truncated to $1000k_0$ to achieve an accuracy better than 1% for the resonance frequencies values. Furthermore, for each examined case, convergence in terms of the number of K and L pivot-vectors is checked, by increasing both K and L to cover sufficiently the spectral space. It has been proved that the $\overline{\underline{G}}_o(\underline{r}, \underline{r}')$ free-space term of the dyadic Greens function appearing in eq. (13) is the most difficult one to converge, compared to the $\overline{\underline{G}}_1(\underline{r}, \underline{r}')$ term associated to the microstrip substrate. To this end, in Tables 4 and 6 this convergence is shown for two indicative cases of an isolated resonator, with a homogeneous distribution of the pivot-vectors in the spectral space. Once the number of the pivot-vectors is large enough to obtain a resonance behaviour, the resonance frequency value is highly converging and does not change by adding more pivots. Nevertheless, the absolute peak values of the corresponding stored electric energy W_e need some increase of the K and/or L values, as shown in Tables 4 and 6, where, as expected, this convergence is even more difficult for electrically larger resonators.

In order to prove the validity of the proposed method, numerical results have been computed and compared with previously published data, concerning dielectric cylindrical resonators, either isolated [9, 12] or mounted on a microstrip substrate [1, 4, 9].

In all the results presented hereafter a cylindrical coordinates system is adopted, with its z-axis coinciding to the cylindrical resonator axis and its $\rho\varphi$-plane coinciding to the ground plane. Then, the excitation

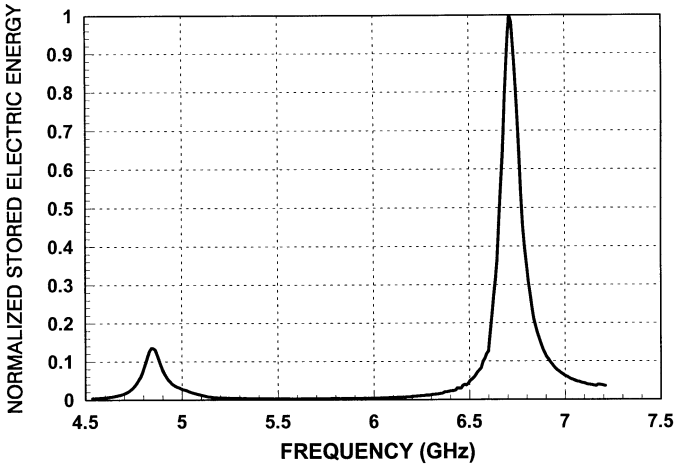

Figure 3. $\mathrm{TE}_{01\delta}$ and $\mathrm{HEM}_{12\delta}$ modes at $f = 4.85\,\mathrm{GHz}$ and $f = 6.66\,\mathrm{GHz}$, respectively for an isolated resonator with $\varepsilon_r = 38$, $\alpha = 5.25\,\mathrm{mm}$ and $d = 4.6\,\mathrm{mm}$.

is considered to be a Hertzian dipole, with electric moment $p_o = 1A{\cdot}m$, orientation $\hat{\delta} = \hat{y}$ and position vector $\underline{r}_o = (x_o, y_o, z_o) = 5\hat{x} + 10\hat{z}$ (in mm). As far as the isolated resonator is concerned, the computations are carried out by considering only the free-space term $\overline{\overline{G}}_o(\underline{r}, \underline{r}')$ in eq. (6). In Figure 3, the resonance behaviour of an isolated cylindrical dielectric resonator is presented, for the two successive resonating modes $\mathrm{TE}_{01\delta}$ and $\mathrm{HEM}_{12\delta}$. As already mentioned, the average stored energy of the electric (or magnetic) field is computed on the frequency axis. Resonant frequencies and linewidths $(1/Q)$ are computed and shown in Table 1, where the comparison with previously reported theoretical and experimental data [12] exhibits a very good agreement.

Further numerical results are presented in Figure 4, concerning another isolated cylindrical dielectric resonator. In Table 2 the results derived by the present analysis are compared with those of [9] and a very good agreement is again exhibited.

Numerical computations have been also carried out for a dielectric cylindrical resonator mounted on a microstrip substrate. First, in Figure 5, a sample case is examined, corresponding to the same resonator as in Figure 4, placed in this case over a metal plate. The distance $(l - h)$ between the metal plate and the resonator is equal to the radius α of the resonator. As shown in Figure 5, the resonant frequency of

MODE	RESONANT FREQUENCY (GHZ)			QUALITY FACTOR		
	MEASURED *[12]*	COMPUTED *Surface Integral Equation [12]*	PRESENT HISTORY	MEASURED *[12]*	COMPUTED *Surface Integral Equation [12]*	PRESENT THEORY
$TE_{01\delta}$	4.85	4.829	4.85	51	45.8	45.2
$HEM_{12\delta}$	6.64	6.638	6.66	64	52.1	59.2

Table 1. Resonant frequency and quality factor for $TE_{01\delta}$ and $HEM_{12\delta}$ modes of an isolated resonator with $\varepsilon_r = 38$, $\alpha = 5.25\,\text{mm}$ and $d = 4.6\,\text{mm}$.

Mode $TE_{01\delta}$	Measured [9]	Computed [9]	Present Theory
Resonant Frequency (GHz)	9.11	9.13	9.14
Quality Factor	46	51	45.75

Table 2. Resonant frequency and quality factor for $TE_{01\delta}$ mode of an isolated resonator with $\varepsilon_r = 38$, $\alpha = 2.86\,\text{mm}$ and $d = 2.38\,\text{mm}$.

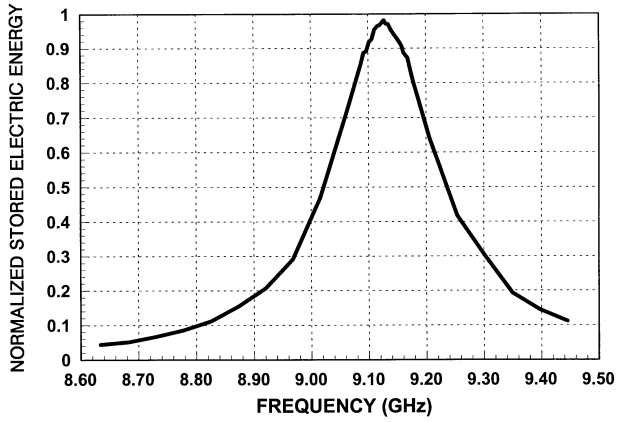

Figure 4. $TE_{01\delta}$ mode for an isolated resonator with $\varepsilon_r = 38$, $\alpha = 2.86\,\text{mm}$ and $d = 2.38\,\text{mm}$.

$TE_{01\delta}$ mode is computed at 9.15 GHz, in agreement to the 9.16 GHz resonant frequency reported in [4]. The quality factor Q has been found to be 185, which is feats to the plot presented in Figure 5 of [9].

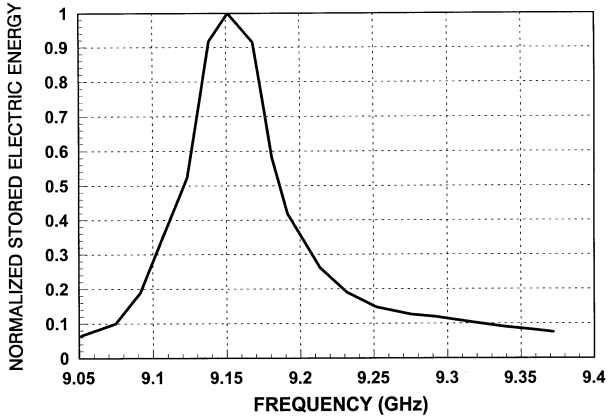

Figure 5. $\mathrm{TE}_{01\delta}$ mode for a resonator with $\varepsilon_r = 38$, $\alpha = 2.86\,\mathrm{mm}$ and $d = 2.38\,\mathrm{mm}$, placed at a distance $l = \alpha(h = 0)$ above a metal plate.

Finally, a second sample of a dielectric cylindrical resonator mounted on a microstrip substrate is examined for comparison purposes. Namely, the $\mathrm{TE}_{01\delta}$ mode for a resonator with $\varepsilon_r = 37.7$, $\alpha = 3.85\,\mathrm{mm}$ and $d = 3.41\,\mathrm{mm}$, mounted on a microstrip substrate with $\varepsilon_{rs} = 2.54$ and thickness $h = 0.254\,\mathrm{mm}$, is shown in Figure 6. The resonant frequency for this mode is reported in pp. 162–163 of [1] to be 7.56 GHz, while, using the present theory, it is computed at 7.58 GHz.

After having checked the validity of the method, new results have been obtained to demonstrate the impact of the resonator height or the presence of the grounded substrate to the resonance properties of the resonator. To this end, first an isolated resonator with $\varepsilon_r = 35$ and radius $\alpha = 3.0\,\mathrm{mm}$ is examined for two different height values $d = 3.0\,\mathrm{mm}$ and $d = 1.5\,\mathrm{mm}$ and second both resonators are mounted on a microstrip substrate with $\varepsilon_{rs} = 2.1$ and thickness $h = 0.69\,\mathrm{mm}$.

The results concerning the $d = 3.0\,\mathrm{mm}$ isolated cylinder are presented in Figure 7 and Table 3, while the results concerning the $d = 1.5\,\mathrm{mm}$ isolated cylinder are presented in Figure 8 and Table 5. Furthermore, for the $d = 1.5\,\mathrm{mm}$ resonator, field distributions are plotted in Figures 9–10, for the $\mathrm{TE}_{01\delta}$ and $\mathrm{HEM}_{12\delta}$ modes respectively, which are in qualitative accordance to Figures 6.16 and 6.30–6.31 of [1]. Comparing Tables 3 and 5, it can be concluded that, as expected, though

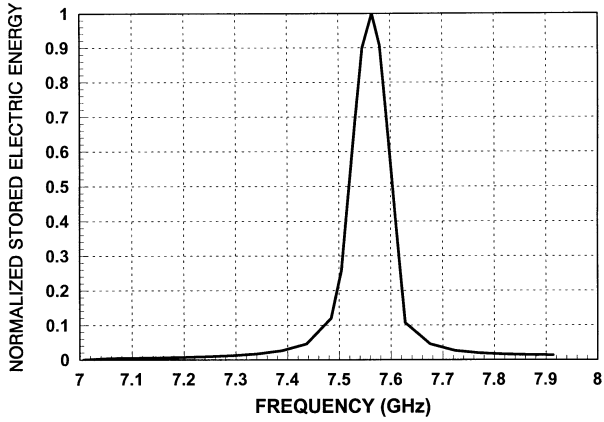

Figure 6. $TE_{01\delta}$ mode for a resonator with $\varepsilon_r = 37.7$, $\alpha = 3.85\,\text{mm}$ and $d = 3.41\,\text{mm}$, mounted on a microstrip substrate with $\varepsilon_{rs} = 2.54$ and thickness $h = 0.254\,\text{mm}$.

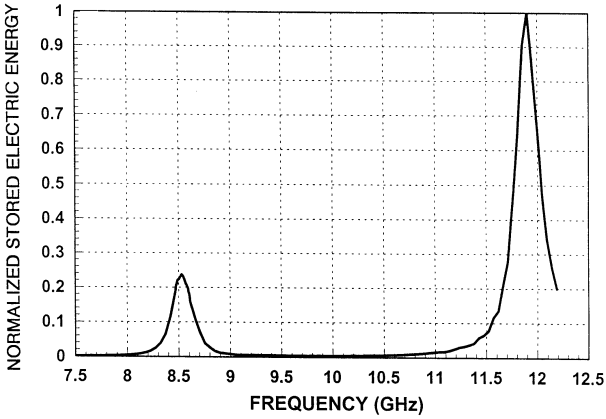

Figure 7. $TE_{01\delta}$ and $HEM_{12\delta}$ modes at $f = 8.565\,\text{GHz}$ and $f = 11.91\,\text{GHz}$, respectively for an isolated resonator with $\varepsilon_r = 35$, $\alpha = 3.0\,\text{mm}$ and $d = 3.0\,\text{mm}$.

Mode	Resonant Frequency (GHz)	Quality Factor
$TE_{01\delta}$	8.565	35.8
$HEM_{12\delta}$	11.91	41.6

Table 3. Resonant frequency and quality factor for $TE_{01\delta}$ and $HEM_{12\delta}$ modes of an isolated resonator with $\varepsilon_r = 35$, $\alpha = 3.00\,\text{mm}$ and $d = 3.00\,\text{mm}$.

K	L	W_e
5	8	521.354
6	8	1204.225
7	8	3329.618
8	8	5496.801
8	10	5547.854
8	12	5601.198
10	10	5609.753
10	12	5598.742

Table 4. Convergence of the absolute peak values of the stored electric energy W_e in terms of the pivot-vectors K and L for $\mathrm{TE}_{01\delta}$ mode of an isolated resonator with $\varepsilon_r = 35$, $\alpha = 3.00\,\mathrm{mm}$ and $d = 3.00\,\mathrm{mm}$.

Mode	Resonant Frequency (GHz)	Quality Factor
$\mathrm{TE}_{01\delta}$	10.57	37.75
$\mathrm{HEM}_{12\delta}$	14.37	42.45

Table 5. Resonant frequency and quality factor for $\mathrm{TE}_{01\delta}$ and $\mathrm{HEM}_{12\delta}$ modes of an isolated resonator with $\varepsilon_r = 35$, $\alpha = 3.00\,\mathrm{mm}$ and $d = 1.50\,\mathrm{mm}$.

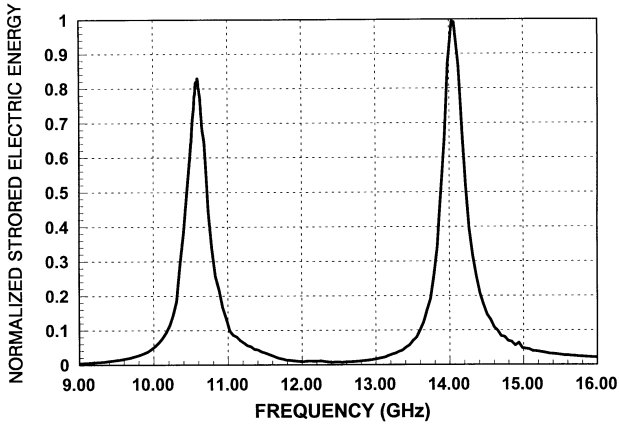

Figure 8. $\mathrm{TE}_{01\delta}$ and $\mathrm{HEM}_{12\delta}$ modes at $f = 10.57\,\mathrm{GHz}$ and $f = 14.37\,\mathrm{GHz}$, respectively for an isolated resonator with $\varepsilon_r = 35$, $\alpha = 3.0\,\mathrm{mm}$ and $d = 1.5\,\mathrm{mm}$.

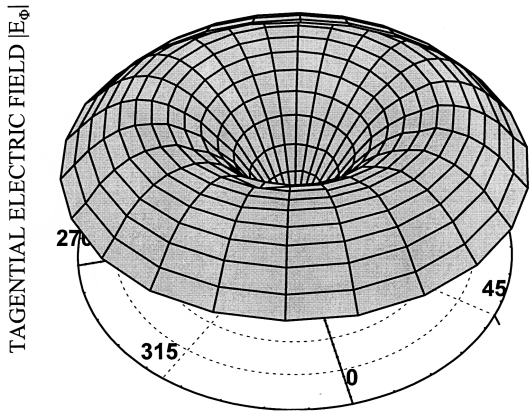

Figure 9. Electric field distribution of the dominant component $|E_\varphi|$ at the equatorial plane $d = 0.75\,\text{mm}$ for $\text{TE}_{01\delta}$ mode of an isolated resonator with $\varepsilon_r = 35$, $\alpha = 3.0\,\text{mm}$ and $d = 1.5\,\text{mm}$.

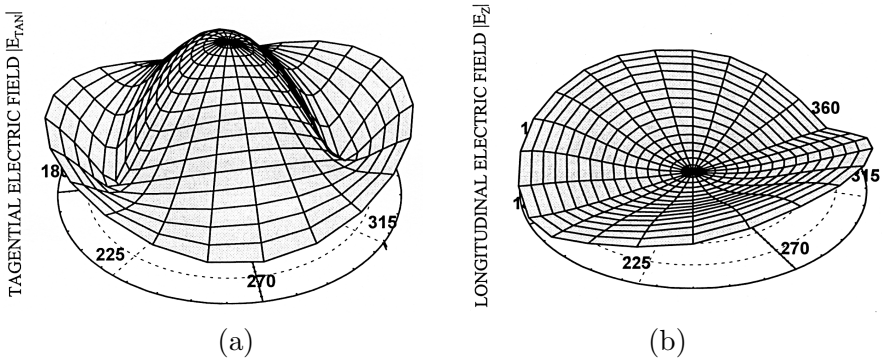

Figure 10. Electric field distribution at the equatorial plane $d = 0.75\,\text{mm}$ for $\text{HEM}_{12\delta}$ mode of an isolated resonator with $\varepsilon_r = 35$, $\alpha = 3.0\,\text{mm}$ and $d = 1.5\,\text{mm}$:
(a) tangential component $|E_{\tan}|$ (b) longitudinal component $|E_z|$.

the quality factor is not affected by the modification of the resonator height, the resonant frequencies are shifted, as predicted by the approximate estimation of eq. (22). Finally, the convergence of the absolute peak values of the corresponding stored electric energy We in terms of the K and L number of pivot-vectors is presented in Tables 4 and 6 respectively for both isolated resonator cases. Note that, since the

K	L	W_e
5	8	494.697
6	8	3605.122
7	8	3329.618
8	8	3362.801
8	10	3346.854
8	12	3407.198
10	10	3397.773
10	12	3385.742

Table 6. Convergence of the absolute peak values of the stored electric energy W_e in terms of the pivot-vectors K and L for $TE_{01\delta}$ mode of an isolated resonator with $\varepsilon_r = 35$, $\alpha = 3.00\,\text{mm}$ and $d = 1.50\,\text{mm}$.

Mode	Resonant Frequency (GHz)	Quality Factor
$TE_{01\delta}$	9.35	143
$HEM_{12\delta}$	12.38	206

Table 7. Resonant frequency and quality factor for $TE_{01\delta}$ and $HEM_{12\delta}$ modes of a resonator with $\varepsilon_r = 35$, $\alpha = 3.00\,\text{mm}$ and $d = 1.50\,\text{mm}$ mounted on a microstrip substrate with $\varepsilon_{rs} = 2.1$ and $h = 0.69$ mm.

$\overline{\underline{G}}_o(\underline{r}, \underline{r}')$ free-space term is the most difficult one to converge, compared to the $\overline{\underline{G}}_1(\underline{r}, \underline{r}')$ term associated to the microstrip substrate, the same number of pivot-vectors needed to solve the isolated resonator problem will also sufficiently cover the spectral space for solving the microstrip substrate mounted resonator problem.

The results concerning the $d = 3.0$ mm cylinder mounted on a microstrip substrate with $\varepsilon_{rs} = 2.1$ and thickness $h = 0.69$ mm are presented in Figure 11 and Table 7, while the results concerning the $d = 1.5$ mm cylinder mounted on the same microstrip substrate are presented in Figure 12 and Table 8. Comparing Table 3 to Table 7 and Table 5 to Table 8, it can be concluded that the presence of the grounded substrate results to a moderate shift of the resonant frequencies, but to an expected significant increase of the quality factor Q. The latter phenomenon, which has been already observed by other

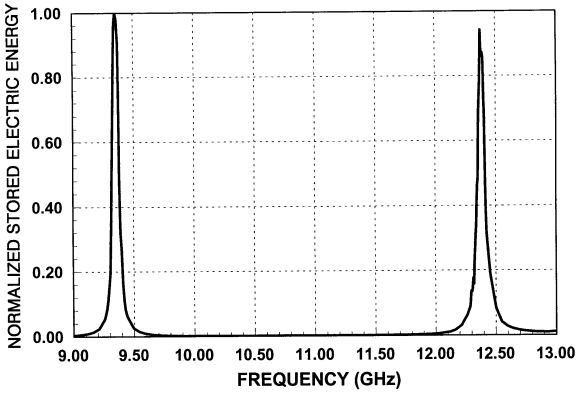

Figure 11. $TE_{01\delta}$ and $HEM_{12\delta}$ modes at $f = 9.35\,\text{GHz}$ and $f = 12.38\,\text{GHz}$, respectively for a resonator with $\varepsilon_r = 35$, $\alpha = 3.0\,\text{mm}$ and $d = 3.0\,\text{mm}$, mounted on a microstrip substrate with $\varepsilon_{rs} = 2.1$ and thickness $h = 0.69\,\text{mm}$.

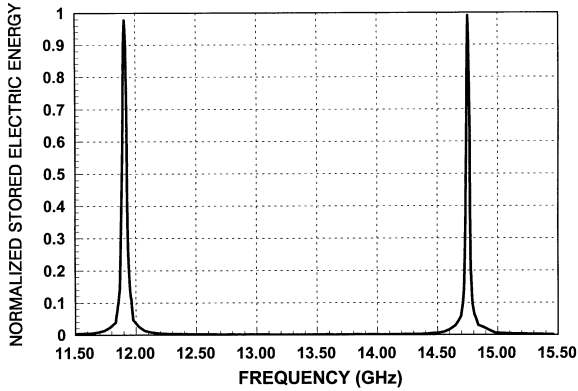

Figure 12. $TE_{01\delta}$ and $HEM_{12\delta}$ modes at $f = 11.91\,\text{GHz}$ and $f = 14.75\,\text{GHz}$, respectively for a resonator with $\varepsilon_r = 35$, $\alpha = 3.0\,\text{mm}$ and $d = 1.5\,\text{mm}$, mounted on a microstrip substrate with $\varepsilon_{rs} = 2.1$ and thickness $h = 0.69\,\text{mm}$.

Mode	**Resonant Frequency (GHz)**	**Quality Factor**
$TE_{01\delta}$	11.91	278
$HEM_{12\delta}$	14.75	476

Table 8. Resonant frequency and quality factor for $TE_{01\delta}$ and $HEM_{12\delta}$ modes of a resonator with $\varepsilon_r = 35$, $\alpha = 3.00\,\text{mm}$ and $d = 3.00\,\text{mm}$ mounted on a microstrip substrate with $\varepsilon_{rs} = 2.1$ and $h = 0.69\,\text{mm}$.

researchers (see Fig. 5 of [9]), is explained by the fact that, when the resonator is placed close to a perfectly conducting surface, the electric field intensity inside the resonator is increased, while the radiation losses are lowered. Furthermore, in case that the conducting surface is covered by a dielectric substrate of low permittivity, no surface waves are excited inside the dielectric substrate, due to the axis-symmetric pattern of the electric field generated by the resonating dielectric cylinder.

Finally, in Figure 13, the variation of the resonant properties of the $d = 1.5$ mm resonator is shown, by moving the resonator with respect to the grounded substrate. As expected, for large distances $(1 - h)$ (approximately five times the resonator height), the isolated resonator solution, given in Table 5, is derived.

6. CONCLUSIONS

A numerically stable and efficient technique to compute the resonance properties of very high permittivity dielectric cylinders placed on a microstrip substrate has been presented. A volume integral equation formulation in conjunction with an entire domain Galerkin technique with a suitable plane wave expansion has been employed and proved to be highly convergent and stable. The computation of the stored average electric (or magnetic) energy inside the dielectric cylinder on the frequency axis has been shown to be an efficient technique to determine the resonance properties of modes with a very high accuracy. Furthermore, the effect of the microstrip substrate to the cylindrical resonator quality factor has been exhibited.

APPENDIX I

The dyadic $\underline{\overline{g}}_1(p_x, p_y) = \underline{\overline{g}}_1(\rho_p, \phi_p)$ appearing in wq. (13) is defined as

$$\underline{\overline{g}}_1(p_x, p_y) = \underline{\overline{g}}_1(\rho_p, \phi_p) = \begin{bmatrix} g_{1xx} & g_{1xy} & g_{1xz} \\ g_{1yx} & g_{1yy} & g_{1xz} \\ g_{1zx} & g_{1zy} & g_{1zz} \end{bmatrix}$$

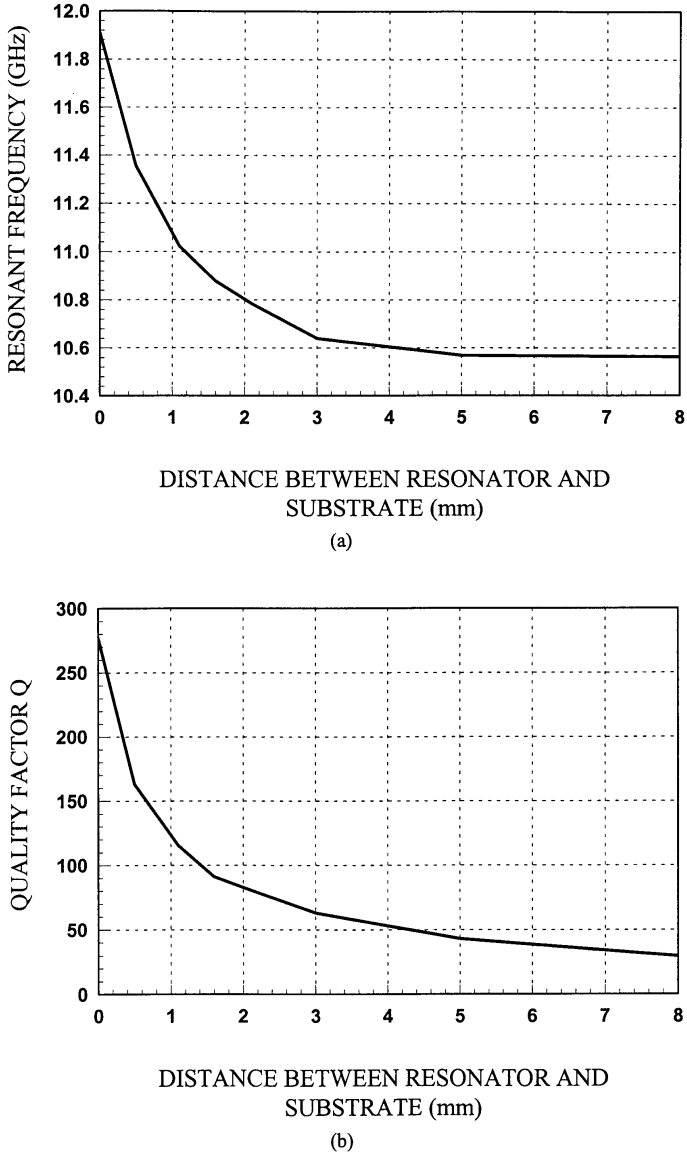

Figure 13. Cylindrical resonator with $\varepsilon_r = 35$, $\alpha = 3.0\,\text{mm}$ and $d = 1.5\,\text{mm}$, placed above a microstrip substrate with $\varepsilon_{rs} = 2.1$ and thickness $h = 0.69\,\text{mm}$: variation of the (a) resonance frequency and (b) quality factor vs. the distance $(1 - h)$ between the resonator and the substrate.

where

$$g_{1xx} = \left[-\left(\frac{k_0^2 - \rho_p^2 \cos^2 \phi_p}{\mu k_0^2} \right) \right.$$
$$\left. + \frac{2(k_0^2 \varepsilon_{rs} - \rho_p^2 \cos^2 \phi_p)(\mu \cos h\mu_1 h + \mu_1 \sin h\mu_1 h) + 2(k_0^2 - \rho_p^2 \cos^2 \phi_p)\mu_1 \sin h^2 \mu_1 h}{k_0^2(\mu\varepsilon_{rs} \cos h\mu_1 h + \mu_1 \sin h\mu_1 h)(\mu_1 \cos h\mu_1 h + \mu \sin h\mu_1 h)} \right]$$

$$g_{1xy} = g_{1yx} = \left[\frac{-2\rho_p^2 \cos\varphi_p \sin\varphi_p \sin h\mu_1 h(\mu \cos h\mu_1 h + \mu_1 \sin h\mu_1 h)}{k_0^2(\mu\varepsilon_{rs} \cos h\mu_1 h + \mu_1 \sin h\mu_1 h)(\mu_1 \cos h\mu_1 h + \mu \sin h\mu_1 h)} \right.$$
$$\left. + \left(\frac{\rho_p^2 \cos\varphi_p \sin\varphi_p}{\mu k_0^2} \right) \right]$$

$$g_{1xz} = -g_{1zx} = \left[\frac{-2i\rho_p \cos\varphi_p \sin h\mu_1 h}{k_o^2(\mu\varepsilon_{rs} \cos h\mu_1 h + \mu_1 \sin h\mu_1 h)} + \left(\frac{i\rho_p \cos\varphi_p}{k_0^2} \right) \right]$$

$$g_{1yy} = \left[-\left(\frac{k_0^2 - \rho_p^2 \sin^2 \phi_p}{\mu k_0^2} \right) \right.$$
$$\left. + \frac{2(k_0^2 \varepsilon_{rs} - \rho_p^2 \sin^2 \phi_p)(\mu \cos h\mu_1 h + \mu_1 \sin h\mu_1 h) + 2(k_0^2 - \rho_p^2 \sin^2 \phi_p)\mu_1 \sin h^2 \mu_1 h}{k_0^2(\mu\varepsilon_{rs} \cos h\mu_1 h + \mu_1 \sin h\mu_1 h)(\mu_1 \cos h\mu_1 h + \mu \sin h\mu_1 h)} \right]$$

$$g_{1yz} = \left[\frac{-2i\rho_p \sin\varphi_p \sin h\mu_1 h}{k_o^2(\mu\varepsilon_{rs} \cos h\mu_1 h + \mu_1 \sin h\mu_1 h)} + \left(\frac{i\rho_p \sin\varphi_p}{k_0^2} \right) \right]$$

$$g_{1zz} = \left[\frac{-2\rho_p^2 \sin h\mu_1 h}{\mu k_0^2(\mu\varepsilon_{rs} \cos h\mu_1 h + \mu_1 \sin h\mu_1 h} + \left(\frac{\mu^2 + k_0^2}{\mu k_0^2} \right) \right]$$

with $\mu = \sqrt{\rho_p^2 - k_0^2}$, $\mu_1 = \sqrt{\rho_p^2 - k_0^2 \varepsilon_{rs}}$, $\mathrm{Re}(\mu) > 0$, $\mathrm{Im}(\mu) < 0$ and $\mathrm{Re}(\mu_1) > 0$, $\mathrm{Im}(\mu_1) < 0$.

APPENDIX II

Eq. (11) is written as

$$\sum_{k=1}^{K}\sum_{l=1}^{L}\begin{bmatrix} K_{xx}(k',l',k,l) & K_{xy}(k',l',k,1) & K_{xz}(k',l',k,1) \\ K_{yx}(k',l',k,1) & K_{yy}(k',l',k,1) & K_{yz}(k',l',k,1) \\ K_{zx}(k',l',k,1) & K_{zy}(k',l',k,1) & K_{zz}(k',l',k,1) \end{bmatrix} \cdot \begin{bmatrix} C_x(k,l) \\ C_y(k,l) \\ C_z(k,l) \end{bmatrix} = \begin{bmatrix} B_x(k',l') \\ B_y(k',l') \\ B_z(k',l') \end{bmatrix}$$

which, according to eq. (13) and retaining the same subscripts denoting the free space and the microstrip substrate impact, is written as

$$\left\{\overline{\underline{K}}_0 + \overline{\underline{K}}_1\right\} \cdot \underline{C} = \hat{\delta} \cdot \left\{\overline{\underline{B}}_0 + \overline{\underline{B}}_1\right\} \Leftrightarrow$$
$$\left\{ \begin{bmatrix} K_{0xx} & K_{0xy} & K_{0xz} \\ K_{0yx} & K_{0yy} & K_{0yz} \\ K_{0zx} & K_{0zy} & K_{0zz} \end{bmatrix} + \begin{bmatrix} K_{1xx} & K_{1xy} & K_{1xz} \\ K_{1yx} & K_{1yy} & K_{1yz} \\ K_{1zx} & K_{1zy} & K_{1zz} \end{bmatrix} \right\} \cdot \begin{bmatrix} C_x \\ C_y \\ C_z \end{bmatrix}$$
$$= \hat{\delta} \cdot \left\{ \begin{bmatrix} B_{0xx} & B_{0xy} & B_{0xz} \\ B_{0yx} & B_{0yy} & B_{0yz} \\ B_{0zx} & B_{0zy} & B_{0zz} \end{bmatrix} + \begin{bmatrix} B_{1xx} & B_{1xy} & B_{1xz} \\ B_{1yx} & B_{1yy} & B_{1yz} \\ B_{1zx} & B_{1zy} & B_{1zz} \end{bmatrix} \right\}$$

Then by denoting

$$k_z = k_0\sqrt{\varepsilon_r}\cos(k\Delta\theta)$$
$$\xi_z = k_0\sqrt{\varepsilon_r}\cos(k'\Delta\theta)$$
$$\underline{\rho}_k = k_0\sqrt{\varepsilon_r}\sin(k\Delta\theta)(\cos(l\Delta\varphi)\hat{x} + \sin(l\Delta\varphi)\hat{y})$$
$$\underline{\rho}_\xi = k_0\sqrt{\varepsilon_r}\sin(k'\Delta\theta)(\cos(l'\Delta\varphi)\hat{x} + \sin(l'\Delta\varphi)\hat{y})$$
$$\underline{\rho}_p = p_x\hat{x} + p_y\hat{y} = \rho_p\hat{\rho}$$

the kernel elements are defined as

$$\overline{\underline{K}}_1 = k_0^2(\varepsilon_r - 1)\int_0^{+\infty} d\rho_p \int_0^{2\pi} d\varphi_p\ \rho_p \left(\frac{\alpha^4 d^2}{2}\right) \left(\frac{J_1\left(|\underline{\rho}_k - \underline{\rho}_p|\alpha\right)}{|\underline{\rho}_k - \underline{\rho}_p|\alpha} \cdot \frac{J_1\left(|\underline{\rho}_p - \underline{\rho}_\xi|\alpha\right)}{|\underline{\rho}_p - \underline{\rho}_\xi|\alpha}\right)$$

$$\frac{\sin\left[(i\mu+k_z)\frac{d}{2}\right]}{(i\mu+k_z)\frac{d}{2}}\,\frac{\sin\left[(i\mu-\xi_z)\frac{d}{2}\right]}{(i\mu-\xi_z)\frac{d}{2}}$$
$$e^{-2\mu d}e^{-2\mu(1-h)}e^{i(k_z-\xi_z)\left(1+\frac{d}{2}\right)}\underline{\overline{g}}_1(\rho_p,\phi_p)$$

with $\underline{\overline{g}}_1(\rho_p,\varphi_r)$ being defined in Appendix I and

$$K_{0_{xx}}=\varepsilon_r 2\pi\alpha^2 d\frac{J_1(|\underline{\rho}_k-\underline{\rho}_\xi|\,\alpha)}{|\underline{\rho}_k-\underline{\rho}_\xi|\,\alpha}\cdot\frac{\sin\left[(k_z-\xi_z)\frac{d}{2}\right]}{(k_z-\xi_z)\frac{d}{2}}\exp^{i(k_z-\xi_z)\left(1+\frac{d}{2}\right)}$$
$$-(\varepsilon_r-1)\alpha^4 d\int_0^{+\infty}d\rho_p\int_0^{2\pi}d\varphi_p\;\rho_p\frac{J_1(|\underline{\rho}_k-\underline{\rho}_p|\,\alpha)}{|\underline{\rho}_k-\underline{\rho}_p|\,\alpha}\cdot$$
$$\cdot\frac{J_1(|\underline{\rho}_\xi-\underline{\rho}_p|\,\alpha)}{|\underline{\rho}_\xi-\underline{\rho}_p|\,\alpha}\;e^{i(k_z-\xi_z)\left(1+\frac{d}{2}\right)}$$
$$\cdot\left\{(k_0^2-\rho_p^2\cos^2\varphi_p)\cdot\left[\frac{1}{\lambda_u}\;\frac{e^{i(\lambda_u-k_z)\frac{d}{2}}}{(\lambda_u-k_z)}\cdot\frac{\sin\left((\lambda_u-\xi_z)\frac{d}{2}\right)}{(\lambda_u-\xi_z)\frac{d}{2}}\right.\right.$$
$$\left.\left.+\frac{1}{\lambda_u}\;\frac{e^{i(\lambda_u+k_z)\frac{d}{2}}}{(\lambda_u+k_z)}\cdot\frac{\sin\left((\lambda_u+\xi_z)\frac{d}{2}\right)}{(\lambda_u+\xi_z)\frac{d}{2}}\right]\right.$$
$$\left.+2[\rho_p^2\sin^2\phi_p+k_z^2]\;\frac{\sin\left[(k_z-\xi_z)\frac{d}{2}\right]}{(k_z-\xi_z)\frac{d}{2}}\cdot\frac{1}{k_z^2-\lambda_u^2}\right\}$$
$$K_{0_{xy}}=K_{o_{yx}}=(\varepsilon_r-1)\alpha^4 d\int_0^{+\infty}d\rho_p\int_0^{2\pi}d\rho_p\;\phi_p\frac{J_1(|\underline{\rho}_k-\underline{\rho}_p|\,\alpha)}{|\underline{\rho}_k-\underline{\rho}_p|\,\alpha}$$
$$\cdot\frac{J_1(|\underline{\rho}_\xi-\underline{\rho}_p|\,\alpha)}{|\underline{\rho}_\xi-\underline{\rho}_p|\,\alpha}\;e^{i(k_z-\xi_z)\left(1+\frac{d}{2}\right)}$$

$$\cdot \left\{ (\rho_p^2 \cos\varphi_p \sin\varphi_p) \cdot \left[\frac{1}{\lambda_u} \frac{e^{i(\lambda_u - k_z)\frac{d}{2}}}{(\lambda_u - k_z)} \cdot \frac{\sin\left((\lambda_u - \xi_z)\frac{d}{2}\right)}{(\lambda_u - \xi_z)\frac{d}{2}} \right.\right.$$

$$\left.\left. + \frac{1}{\lambda_u} \frac{e^{i(\lambda_u + k_z)\frac{d}{2}}}{(\lambda_u + k_z)} \cdot \frac{\sin\left((\lambda_u + \xi_z)\frac{d}{2}\right)}{(\lambda_u + \xi_z)\frac{d}{2}} \right] \right.$$

$$\left. + 2 \frac{\sin\left[(k_z - \xi_z)\frac{d}{2}\right]}{(k_z - \xi_z)\frac{d}{2}} \cdot \frac{1}{k_z^2 - \lambda_u^2} \right\}$$

$$K_{0_{xz}} = K_{o_{zx}} = (\varepsilon_r - 1)\alpha^4 d \int_0^{+\infty} d\rho_p \int_0^{2\pi} d\varphi_p \ \rho_p \frac{J_1(|\underline{\rho}_k - \underline{\rho}_p| \ \alpha)}{|\underline{\rho}_k - \underline{\rho}_p| \ \alpha}$$

$$\cdot \frac{J_1(|\underline{\rho}_\xi - \underline{\rho}_p| \ \alpha)}{|\underline{\rho}_\xi - \underline{\rho}_p| \ \alpha} \ e^{i(k_z - \xi_z)\left(1 + \frac{d}{2}\right)}$$

$$\cdot \left\{ (\lambda_u - \ _p \cos\varphi_p) \cdot \left[\frac{1}{\lambda_u} \frac{e^{i(\lambda_u - k_z)\frac{d}{2}}}{(\lambda_u - k_z)} \cdot \frac{\sin\left((\lambda_u - \xi_z)\frac{d}{2}\right)}{(\lambda_u - \xi_z)\frac{d}{2}} \right.\right.$$

$$\left.\left. - \frac{1}{\lambda_u} \frac{e^{i(\lambda_u + k_z)\frac{d}{2}}}{(\lambda_u + k_z)} \cdot \frac{\sin\left((\lambda_u + \xi_z)\frac{d}{2}\right)}{(\lambda_u + \xi_z)\frac{d}{2}} \right] \right.$$

$$\left. + 2k_z\rho_p \frac{\sin\left[(k_z - \xi_z)\frac{d}{2}\right]}{(k_z - \xi_z)\frac{d}{2}} \cdot \frac{1}{k_z^2 - \lambda_u^2} \right\}$$

$$K_{0_{yy}} = \varepsilon_r 2\pi\alpha^2 d \frac{J_1(|\underline{\rho}_k - \underline{\rho}_\xi| \ \alpha)}{|\underline{\rho}_k - \underline{\rho}_\xi| \ \alpha} \cdot \frac{\sin\left[(k_z - \xi_z)\frac{d}{2}\right]}{(k_z - \xi_z)\frac{d}{2}} e^{i(k_z - \xi_z)\left(1 + \frac{d}{2}\right)}$$

$$- (\varepsilon_r - 1)\alpha^4 d \int_0^{+\infty} d\rho_p \int_0^{2\pi} d\varphi_p \ \rho_p \frac{J_1(|\underline{\rho}_k - \underline{\rho}_p| \ \alpha)}{|\underline{\rho}_k - \underline{\rho}_p| \ \alpha}$$

$$\cdot \frac{J_1(|\underline{\rho}_\xi - \underline{\rho}_p|\ \alpha)}{|\underline{\rho}_\xi - \underline{\rho}_p|\ \alpha}\ e^{i(k_z-\xi_z)\left(1+\frac{d}{2}\right)}$$

$$\cdot \left\{ (k_0^2 - \rho_p^2 \sin^2\phi_p) \cdot \left[\frac{1}{\lambda_u}\ \frac{e^{i(\lambda_u - k_z)\frac{d}{2}}}{(\lambda_u - k_z)} \cdot \frac{\sin\left((\lambda_u - \xi_z)\frac{d}{2}\right)}{(\lambda_u - \xi_z)\frac{d}{2}} \right.\right.$$

$$\left.\left. + \frac{1}{\lambda_u}\ \frac{e^{i(\lambda_u + k_z)\frac{d}{2}}}{(\lambda_u + k_z)} \cdot \frac{\sin\left((\lambda_u + \xi_z)\frac{d}{2}\right)}{(\lambda_u + \xi_z)\frac{d}{2}} \right] \right.$$

$$\left. + [\rho_p^2 \cos^2\phi_p + k_z^2]\ \frac{\sin\left[(k_z - \xi_z)\frac{d}{2}\right]}{(k_z - \xi_z)\frac{d}{2}} \cdot \frac{1}{k_z^2 - \lambda_u^2} \right\}\ 2$$

$$K_{0_{yz}} = K_{0_{zy}} = (\varepsilon_r - 1)\alpha^4 d \int_0^{+\infty} d\rho_p \int_0^{2\pi} d\varphi_p\ \rho_p \frac{J_1(|\underline{\rho}_k - \underline{\rho}_p|\ \alpha)}{|\underline{\rho}_k - \underline{\rho}_p|\ \alpha}$$

$$\cdot \frac{J_1(|\underline{\rho}_\xi - \underline{\rho}_p|\ \alpha)}{|\underline{\rho}_\xi - \underline{\rho}_p|\ \alpha}\ e^{i(k_z-\xi_z)\left(1+\frac{d}{2}\right)}$$

$$\cdot \left\{ (\lambda_u \rho_p \sin\varphi_p) \cdot \left[\frac{1}{\lambda_u}\ \frac{e^{i(\lambda_u - k_z)\frac{d}{2}}}{(\lambda_u - k_z)} \cdot \frac{\sin\left((\lambda_u - \xi_z)\frac{d}{2}\right)}{(\lambda_u - \xi_z)\frac{d}{2}} \right.\right.$$

$$\left.\left. - \frac{1}{\lambda_u}\ \frac{e^{i(\lambda_u + k_z)\frac{d}{2}}}{(\lambda_u + k_z)} \cdot \frac{\sin\left((\lambda_u + \xi_z)\frac{d}{2}\right)}{(\lambda_u + \xi_z)\frac{d}{2}} \right] \right.$$

$$\left. + 2k_z\rho_p\ \frac{\sin\left[(k_z - \xi_z)\frac{d}{2}\right]}{(k_z - \xi_z)\frac{d}{2}} \cdot \frac{1}{k_z^2 - \lambda_u^2} \right\}$$

$$K_{0_{zz}} = \varepsilon_r 2\pi\alpha^2 d \frac{J_1(|\underline{\rho}_k - \underline{\rho}_\xi|\ \alpha)}{|\underline{\rho}_k - \underline{\rho}_\xi|\ \alpha} \cdot \frac{\sin\left[(k_z - \xi_z)\frac{d}{2}\right]}{(k_z - \xi_z)\frac{d}{2}} e^{i(k_z-\xi_z)\left(1+\frac{d}{2}\right)}$$

$$
\begin{aligned}
&- (\varepsilon_r - 1)\alpha^4 d \int_0^{+\infty} d\rho_p \int_0^{2\pi} d\varphi_p \; \rho_p \frac{J_1(|\underline{\rho}_k - \underline{\rho}_p|\; \alpha)}{|\underline{\rho}_k - \underline{\rho}_p|\; \alpha} \\
&\cdot \frac{J_1(|\underline{\rho}_\xi - \underline{\rho}_p|\; \alpha)}{|\underline{\rho}_\xi - \underline{\rho}_p|\; \alpha} \; e^{i(k_z - \xi_z)\left(1 + \frac{d}{2}\right)} \\
&\cdot \left\{ \rho_p^2 \left[\frac{1}{\lambda_u} \; \frac{e^{i(\lambda_u - k_z)\frac{d}{2}}}{(\lambda_u - k_z)} \cdot \frac{\sin\left((\lambda_u - \xi_z)\frac{d}{2}\right)}{(\lambda_u - \xi_z)\frac{d}{2}} \right.\right. \\
&+ \frac{1}{\lambda_u} \; \frac{e^{i(\lambda_u + k_z)\frac{d}{2}}}{(\lambda_u + k_z)} \cdot \frac{\sin\left((\lambda_u + \xi_z)\frac{d}{2}\right)}{(\lambda_u + \xi_z)\frac{d}{2}} \\
&\left.\left. + 2 \; \frac{\sin\left[(k_z - \xi_z)\frac{d}{2}\right]}{(k_z - \xi_z)\frac{d}{2}} \cdot \frac{1}{k_z^2 - \lambda_u^2} \right] \right\} .
\end{aligned}
$$

The right-hand terms $\overline{\underline{B}}_1$ are defined as

$$
\begin{aligned}
\overline{\underline{B}}_1 = &\int_0^{+\infty} d\rho_p \int_0^{2\pi} d\phi_p \; \rho_p \left(\frac{\alpha^4 d^2}{2}\right) \left(\frac{J_1(|\underline{\rho}_p - \underline{\rho}_\xi|\; \alpha)}{|\underline{\rho}_p - \underline{\rho}_\xi|\; \alpha}\right) \cdot \\
&\cdot \frac{\sin\left[(i\mu - \xi_z)\frac{d}{2}\right]}{(i\mu - \xi_z)\frac{d}{2}} \; e^{-2\mu h} \; e^{i(i\mu - \xi_z)\left(1 + \frac{d}{2}\right)} e^{-i\rho_p \rho_0 \cos(\phi_p - \phi_0)} e^{-\mu z_0} \overline{\underline{g}}_1(\rho_p, \; \phi_p)
\end{aligned}
$$

while for the right-hand terms $\overline{\underline{B}}_0$ three different cases appear, depending on the z-coordinate of the excitation source point (x_0, y_0, z_0):

i) for $1 + d - z_0 > 0$ and $1 - z_0 > 0$

$$
\begin{aligned}
B_{0xx} = &\left(\frac{\alpha}{2\pi k_0}\right)^2 \int_0^{+\infty} d\rho_p \int_0^{2\pi} d\varphi_p \; \rho_p \; \frac{J_1(|\underline{\rho}_\xi - \underline{\rho}_p|\; \alpha)}{|\underline{\rho}_\xi - \underline{\rho}_p|\; \alpha} \cdot e^{-i\rho_p \rho_0 \cos(\phi_p - \phi_0)} \\
&\left\{ (k_0^2 - \rho_p^2 \cos^2 \phi_p) \cdot \frac{\pi}{\lambda_u} \left(\frac{e^{i\lambda_u(1 + d - z_0) - i\mu_z(1 + d)} - e^{i\lambda_u(1 - z_0) - i\xi_z 1}}{(\lambda_u - \xi_z)} \right) \right\}
\end{aligned}
$$

$$B_{0xy} = B_{0yx}$$

$$= -\left(\frac{\alpha}{2\pi k_0}\right)^2 \int_0^{+\infty} d\rho_p \int_0^{2\pi} d\varphi_p \ \rho_p \ \frac{J_1(|\underline{\rho}_\xi - \underline{\rho}_p| \ \alpha)}{|\underline{\rho}_\xi - \underline{\rho}_p| \ \alpha} \ \cdot e^{-i\rho_p\rho_0\cos(\phi_p-\phi_0)}$$

$$\left\{\rho_p^2 \sin\phi_p \cos\phi_p) \cdot \frac{\pi}{\lambda_u}\left(\frac{e^{i\lambda_u(1+d-z_0)-i\xi_z(1+d)} - e^{i\lambda_u(1-z_0)-i\xi_z 1}}{(\lambda_u - \xi_z)}\right)\right\}$$

$$B_{0xz} = B_{0zx}$$

$$= -\left(\frac{\alpha}{2\pi k_0}\right)^2 \int_0^{+\infty} d\rho_p \int_0^{2\pi} d\phi_p \ \rho_p \ \frac{J_1(|\underline{\rho}_\xi - \underline{\rho}_p| \ \alpha)}{|\underline{\rho}_\xi - \underline{\rho}_p| \ \alpha} \ \cdot e^{-i\rho_p\rho_0\cos(\phi_p-\phi_0)}$$

$$\left\{\rho_p \cos\phi_p) \cdot \pi \ \left(\frac{e^{i\lambda_u(1+d-z_0)-i\xi_z(1+d)} - e^{i\lambda_u(1-z_0)-i\xi_z 1}}{(\lambda_u - \xi_z)}\right)\right\}$$

$$B_{0yy} = \left(\frac{\alpha}{2\pi k_0}\right)^2 \int_0^{+\infty} d\rho_p \int_0^{2\pi} d\varphi_p \ \rho_p \ \frac{J_1(|\underline{\rho}_\xi - \underline{\rho}_p| \ \alpha)}{|\underline{\rho}_\xi - \underline{\rho}_p| \ \alpha} \ \cdot e^{-i\rho_p\rho_0\cos(\varphi_p-\varphi_0)}$$

$$\left\{(k_0^2 - \rho_p^2 \sin^2\phi_p) \cdot \frac{\pi}{\lambda_u}\left(\frac{e^{i\lambda_u(1+d-z_0)-i\xi_z(1+d)} - e^{i\lambda_u(1-z_0)-i\xi_z 1}}{(\lambda_u - \xi_z)}\right)\right\}$$

$$B_{0yz} = B_{0zy}$$

$$= -\left(\frac{\alpha}{2\pi k_0}\right)^2 \int_0^{+\infty} d\rho_p \int_0^{2\pi} d\phi_p \ \rho_p \ \frac{J_1(|\underline{\rho}_\xi - \underline{\rho}_p| \ \alpha)}{|\underline{\rho}_\xi - \underline{\rho}_p| \ \alpha} \ \cdot e^{-i\rho_p\rho_0\cos(\phi_p-\phi_0)}$$

$$\left\{\rho_p \sin\varphi_p) \cdot \pi \ \left(\frac{e^{i\lambda_u(1+d-z_0)-i\xi_z(1+d)} - e^{i\lambda_u(1-z_0)-i\xi_z 1}}{(\lambda_u - \xi_z)}\right)\right\}$$

$$B_{0zz} = \left(\frac{\alpha}{2\pi k_o}\right)^2 \int_0^{+\infty} d\rho_p \int_0^{2\pi} d\varphi_p \ \rho_p \ \frac{J_1(|\underline{\rho}_\xi - \underline{\rho}_p| \ \alpha)}{|\underline{\rho}_\xi - \underline{\rho}_p| \ \alpha} \ \cdot e^{-i\rho_p\rho_o\cos(\phi_p-\phi_o)}$$

$$\left\{(k_0^2 - \rho_p^2 \cos^2\phi_p) \cdot \frac{\pi}{\lambda_u}\left(\frac{e^{i\lambda_u(1+d-z_0)-i\xi_z(1+d)} - e^{i\lambda_u(1-z_0)-i\xi_z 1}}{(\lambda_u - \xi_z)}\right)\right\}$$

ii) for $1 + d - z_0 > 0$ and $1 - z_0 < 0$

$$B_{0xx} = \left(\frac{\alpha}{2\pi k_0}\right)^2 \int_0^{+\infty} d\rho_p \int_0^{2\pi} d\varphi_p \ \rho_p \ \frac{J_1(|\underline{\rho}_\xi - \underline{\rho}_p| \ \alpha)}{|\underline{\rho}_\xi - \underline{\rho}_p| \ \alpha} \ \cdot e^{-i\rho_p\rho_0\cos(\phi_p-\phi_0)}$$

$$\left\{(k_0^2-\rho_p^2\cos^2\phi_p)\cdot\frac{\pi}{\lambda_u}\left(\frac{e^{i\lambda_u(1+d-z_0)-i\xi_z(1+d)}}{(\lambda_u-\xi_z)}\right.\right.$$
$$\left.\left.+\ \frac{e^{i\lambda_u(1-z_o)-i\xi_z 1}}{(\lambda_u+\xi_z)}\right)+2\pi\ \frac{e^{i\lambda_z z_0}}{\xi_z^2-\lambda_u^2}\right\}$$

$$B_{0xy}=B_{0yx}$$
$$=-\left(\frac{\alpha}{2\pi k_0}\right)^2\int_0^{+\infty}d\rho_p\int_0^{2\pi}d\varphi_p\ \rho_p\ \frac{J_1(|\underline{\rho}_\xi-\underline{\rho}_p|\ \alpha)}{|\underline{\rho}_\xi-\underline{\rho}_p|\ \alpha}\ \cdot e^{-i\rho_p\rho_0\cos(\phi_p-\phi_0)}$$
$$\left\{\rho_p^2\sin\phi_p\cos\phi_p)\cdot\frac{\pi}{\lambda_u}\left(\frac{e^{i\lambda_u(1+d-z_0)-i\xi_z(1+d)}}{(\lambda_u-\xi_z)}\right.\right.$$
$$\left.\left.+\ \frac{e^{i\lambda_u(1-z_0)-i\xi_z 1}}{(\lambda_u+\xi_z)}\right)+2\pi\ \frac{e^{i\lambda_z z_0}}{\xi_z^2-\lambda_u^2}\right\}$$

$$B_{0xz}=B_{0zx}$$
$$=-\left(\frac{\alpha}{2\pi k_0}\right)^2\int_0^{+\infty}d\rho_p\int_0^{2\pi}d\phi_p\ \rho_p\ \frac{J_1(|\underline{\rho}_\xi-\underline{\rho}_p|\ \alpha)}{|\underline{\rho}_\xi-\underline{\rho}_p|\ \alpha}\ \cdot e^{-i\rho_p\rho_0\cos(\phi_p-\phi_0)}$$
$$\left\{\rho_p\cos\phi_p)\cdot\pi\ \left(\frac{e^{i\lambda_u(1+d-z_0)-i\xi_z(1+d)}}{(\lambda_u-\xi_z)}\right.\right.$$
$$\left.\left.+\ \frac{e^{i\lambda_u(1-z_0)-i\xi_z 1}}{(\lambda_u+\xi_z)}\right)+2\pi\ \frac{e^{i\lambda_z z_0}}{\xi_z^2-\lambda_u^2}\right\}$$

$$B_{0yy}=\left(\frac{\alpha}{2\pi k_0}\right)^2\int_0^{+\infty}d\rho_p\int_0^{2\pi}d\varphi_p\ \rho_p\ \frac{J_1(|\underline{\rho}_\xi-\underline{\rho}_p|\ \alpha)}{|\underline{\rho}_\xi-\underline{\rho}_p|\ \alpha}\ \cdot e^{-i\rho_p\rho_0\cos(\varphi_p-\varphi_0)}$$
$$\left\{(k_0^2-\rho_p^2\sin^2\phi_p)\cdot\frac{\pi}{\lambda_u}\left(\frac{e^{i\lambda_u(1+d-z_0)-i\xi_z(1+d)}}{(\lambda_u-\xi_z)}\right.\right.$$
$$\left.\left.+\ \frac{e^{i\lambda_u(1-z_0)-i\xi_z 1}}{(\lambda_u+\xi_z)}\right)+2\pi\ \frac{e^{i\lambda_z z_0}}{\xi_z^2-\lambda_u^2}\right\}$$

$$B_{0yz}=B_{0zy}$$
$$=-\left(\frac{\alpha}{2\pi k_o}\right)^2\int_0^{+\infty}d\rho_p\int_0^{2\pi}d\phi_p\ \rho_p\ \frac{J_1(|\underline{\rho}_\xi-\underline{\rho}_p|\ \alpha)}{|\underline{\rho}_\xi-\underline{\rho}_p|\ \alpha}\ \cdot e^{-i\rho_p\rho_0\cos(\phi_p-\phi_0)}$$

$$\left\{\rho_p \sin\varphi_p) \cdot \pi \left(\frac{e^{i\lambda_u(1+d-z_0)-i\xi_z(1+d)}}{(\lambda_u-\xi_z)} + \frac{e^{i\lambda_u(1-z_0)-i\xi_z 1}}{(\lambda_u+\xi_z)}\right) + 2\pi \frac{e^{i\lambda_z z_0}}{\xi_z^2-\lambda_u^2}\right\}$$

$$B_{0zz} = \left(\frac{\alpha}{2\pi k_0}\right)^2 \int_0^{+\infty} d\rho_p \int_0^{2\pi} d\varphi_p \ \rho_p \ \frac{J_1(|\underline{\rho}_\xi - \underline{\rho}_p|\ \alpha)}{|\underline{\rho}_\xi - \underline{\rho}_p|\ \alpha} \cdot e^{-i\rho_p\rho_0\cos(\phi_p-\phi_0)}$$

$$\left\{(k_0^2-\rho_p^2\cos^2\phi_p) \cdot \frac{\pi}{\lambda_u}\left(\frac{e^{i\lambda_u(1+d-z_0)-i\xi_z(1+d)}}{(\lambda_u-\xi_z)} + \frac{e^{i\lambda_u(1-z_0)-i\xi_z 1}}{(\lambda_u+\xi_z)}\right) + 2\pi \frac{e^{i\lambda_z z_0}}{\xi_z^2-\lambda_u^2}\right\}$$

iii) for $1+d-z_0<0$ and $1-z_o<0$

$$B_{0xx} = \left(\frac{\alpha}{2\pi k_o}\right)^2 \int_0^{+\infty} d\rho_p \int_0^{2\pi} d\varphi_p \ \rho_p \ \frac{J_1(|\underline{\rho}_\xi - \underline{\rho}_p|\ \alpha)}{|\underline{\rho}_\xi - \underline{\rho}_p|\ \alpha} \cdot e^{-i\rho_p\rho_0\cos(\phi_p-\phi_o)}$$

$$\left\{(k_o^2-\rho_p^2\cos^2\phi_p) \cdot \frac{\pi}{\lambda_u}\left(\frac{e^{-i\lambda_u(1-z_0)-i\xi_z 1}}{(\lambda_u+\xi_z)} - \frac{e^{-i\lambda_u(1+d-z_o)-i\xi_z(1+d)}}{(\lambda_u+\xi_z)}\right)\right\}$$

$$B_{0xy} = B_{0yx}$$

$$= -\left(\frac{\alpha}{2\pi k_0}\right)^2 \int_0^{+\infty} d\rho_p \int_0^{2\pi} d\varphi_p \ \rho_p \ \frac{J_1(|\underline{\rho}_\xi - \underline{\rho}_p|\ \alpha)}{|\underline{\rho}_\xi - \underline{\rho}_p|\ \alpha} \cdot e^{-i\rho_p\rho_0\cos(\phi_p-\phi_0)}$$

$$\left\{\rho_p^2 \sin\phi_p\cos\phi_p) \cdot \frac{\pi}{\lambda_u}\left(\frac{e^{-i\lambda_u(1-z_0)-i\xi_z 1} - e^{-i\lambda_u(1+d-z_0)-i\xi_z(1+d)}}{(\lambda_u+\xi_z)}\right)\right\}$$

$$B_{0xz} = B_{0zx}$$

$$= -\left(\frac{\alpha}{2\pi k_0}\right)^2 \int_0^{+\infty} d\rho_p \int_0^{2\pi} d\phi_p \ \rho_p \ \frac{J_1(|\underline{\rho}_\xi - \underline{\rho}_p|\ \alpha)}{|\underline{\rho}_\xi - \underline{\rho}_p|\ \alpha} \cdot e^{-i\rho_p\rho_0\cos(\phi_p-\phi_0)}$$

$$\left\{\rho_p\cos\phi_p) \cdot \pi \left(\frac{e^{-i\lambda_u(1-z_0)-i\xi_z 1} - e^{-i\lambda_u(1+d-z_0)-i\xi_z(1+d)}}{(\lambda_u+\xi_z)}\right)\right\}$$

$$B_{0yy} = \left(\frac{\alpha}{2\pi k_0}\right)^2 \int_0^{+\infty} d\rho_p \int_0^{2\pi} d\varphi_p \ \rho_p \ \frac{J_1(|\underline{\rho}_\xi - \underline{\rho}_p| \ \alpha)}{|\underline{\rho}_\xi - \underline{\rho}_p| \ \alpha} \ \cdot e^{-i\rho_p\rho_0\cos(\varphi_p - \varphi_0)}$$

$$\left\{(k_0^2 - \rho_p^2 \sin^2\phi_p) \cdot \frac{\pi}{\lambda_u}\left(\frac{e^{-i\lambda_u(1-z_0)-i\xi_z 1} - e^{-i\lambda_u(1+d-z_0)-i\xi_z(1+d)}}{(\lambda_u + \xi_z)}\right)\right\}$$

$$B_{0yz} = B_{0zy}$$

$$= -\left(\frac{\alpha}{2\pi k_0}\right)^2 \int_0^{+\infty} d\rho_p \int_0^{2\pi} d\phi_p \ \rho_p \ \frac{J_1(|\underline{\rho}_\xi - \underline{\rho}_p| \ \alpha)}{|\underline{\rho}_\xi - \underline{\rho}_p| \ \alpha} \ \cdot e^{-i\rho_p\rho_0\cos(\phi_p - \phi_0)}$$

$$\left\{\rho_p \sin\varphi_p) \cdot \pi \ \left(\frac{e^{-i\lambda_u(1-z_0)-i\xi_z 1} - e^{-i\lambda_u(1+d-z_0)-i\xi_z(1+d)}}{(\lambda_u + \xi_z)}\right)\right\}$$

$$B_{0zz} = \left(\frac{\alpha}{2\pi k_0}\right)^2 \int_0^{+\infty} d\rho_p \int_0^{2\pi} d\varphi_p \ \rho_p \ \frac{J_1(|\underline{\rho}_\xi - \underline{\rho}_p| \ \alpha)}{|\underline{\rho}_\xi - \underline{\rho}_p| \ \alpha} \ \cdot e^{-i\rho_p\rho_0\cos(\phi_p - \phi_0)}$$

$$\left\{(k_0^2 - \rho_p^2 \cos^2\phi_p) \cdot \frac{\pi}{\lambda_u}\left(\frac{e^{-i\lambda_u(1-z_0)-i\xi_z 1} - e^{-i\lambda_u(1+d-z_0)-i\xi_z(1+d)}}{(\lambda_u + \xi_z)}\right)\right\}$$

REFERENCES

1. Butler, C., "General analysis of a narrow slot in a conducting screen between half-spaces of different electromagnetic properties," *Radio Sci.,* Vol. 22, No. 7, 1149–1154, 1987.
2. Chammeloux, L., C. Pichot, and J. C. Bolomey, "Electromagnetic modeling for microwave imaging of cylindrical buried inhomogeneities," *IEEE Trans. Microwave Theory Tech,* Vol. 34, No. 10, 1064–1076, 1986.
3. Kong, J. A., *Electromagnetic Wave Theory,* Wiley-Interscience, New York, 1986.
1. Kajfez, D. and P. Guillon, Eds., *Dielectric Resonators,* Norwood, MA: Artech House, 1986.
2. Cohn, S. B., "Microwave bandpass filters containing high-Q dielectric resonators," *IEEE Trans. Microwave Theory Tech.,* Vol. MTT-16, 218–227, 1968.
3. Itoh, T. and R. S. Rudokas, "New methods for computing the resonant frequencies of dielectric resonators," *IEEE Trans. Microwave Theory Tech.,* Vol. MTT-25, 52–54, 1977.

4. Mongia, R. K., "Resonant frequency of cylindrical dielectric resonator placed in an MIC environment," *IEEE Trans. Microwave Theory Tech.,* Vol. MTT-38, 802–804, 1990.
5. Mongia, R. K. and P. Bhartia, "Accurate conductor Q-factor of dielectric resonator placed in an MIC environment," *IEEE Trans. Microwave Theory Tech.,* Vol. MTT-41, 445–449, 1993.
6. Gelin, P., S. Toutain, P. Kennis, and J. Citerne, "Scattering of the TE01 and TM01 modes on transverse discontinuities in a rod dielectric waveguide - application to the dielectric resonators," *IEEE Trans. Microwave Theory Tech.,* Vol. MTT-29, 712–719, 1981.
7. Komatsu, Y. and Y. Murakami, "Coupling coefficient between microstrip line and dielectric resonator," *IEEE Trans. Microwave Theory Tech.,* Vol. MTT-31, 34–40, 1983.
8. Tsuji, M., H. Shigesawa, and K. Takiyama, "On the complex resonator frequency of open dielectric resonators," *IEEE Trans. Microwave Theory Tech.,* Vol. MTT-31, 392–396, 1983.
9. Tsuji, M., H. Shigesawa, and K. Takiyama, "Analytical and experimental investigations on several resonant modes in open dielectric resonators," *IEEE Trans Microwave Theory Tech.,* Vol. MTT-32, 628–633, 1984.
10. Zaki, K. A. and C. Chen, "New results in dielectric-loaded resonators," *IEEE Trans. Microwave Theory Tech.,* Vol. MTT-34, 815–825, 1986.
11. Jaworski, M. and M. W. Pospieszalski, "An accurate solution of the cylindrical dielectric resonator problem", *IEEE Trans. Microwave Theory Tech.,* Vol. MTT-27, 639–643, 1979.
12. Glisson, A. W., D. Kaifez, and J. James, "Evaluation of modes in dielectric resonators using a surface integration equation formulation," *IEEE Trans. Microwave Theory Tech.,* Vol. MTT-31, 1023–1029, 1983.
13. Kishk, A. A., H. A. Auda, and B. C. Ahn, "Radiation characteristics of cylindrical dielectric resonator antenna with new applications," *IEEE Antennas Propagat. Soc. Newsletter,* Vol. 31, 7–16, 1989.
14. Kishk, A. A., M. R. Zunoubi, and D. Kajfez, "A numerical study of a dielectric disk antenna above grounded dielectric substrate," *IEEE Trans. Antennas Propagat.,* Vol. AP-41, 813–821, 1993.
15. Yousefi, M. and S. K. Chaudhuri, "Dielectric resonator-microstrip interactive circuit analysis and design using integral equation techniques," *IEEE Trans. Microwave Theory Tech.,* Vol. MTT-43, 1446–1452, 1995.

16. Yousefi, M., S. K. Chaudhuri, and S. Safavi-Naeini, "GIBC formulation for the resonant frequencies and field distribution of a substrate-mounted dielectric resonator," *IEEE Trans. Antennas Propagat.,* Vol. AP-42, 38–46, 1994.
17. Gil, F. H. and J. P. Martinez, "Analysis of dielectric resonators with tuning screw and supporting structure," *IEEE Trans. Microwave Theory Tech.,* Vol. MTT-33, 1453–1457, 1985.
18. Su, C. C. and J. M. Guan, "Finite-difference analysis of dielectric-loaded cavities using the simultaneous iteration of the power method with the Chebyshev acceleration technique," *IEEE Trans. Microwave Theory Tech.,* Vol. MTT-42, 1998–2006, 1994.
19. Guan, J. M. and C. C. Su, "Precise computations of resonant frequencies and quality factors for dielectric resonators in MICs with tuning elements," *IEEE Trans. Microwave Theory Tech.,* Vol. MTT-45, 439–442, 1997.
20. Navarro, A. and M. J. Nunez, "FDTD method coupled with FFT: A generalization to open cylindrical devices," *IEEE Trans. Microwave Theory Tech.,* Vol. MTT-42, 870–874, 1994.
21. Pereda, J. A., L. A. Vielva, A. Vegas, and A. Prieto, "Computation of resonant frequencies and quality factors of open dielectric resonators by a combination of the finite-difference time-domain (FDTD) and pronys methods," *IEEE Microwave Guided Wave Lett.,* Vol. 2, 431–433, 1992.
22. Van Bladel, J., "On the resonances of a dielectric resonator of very high permittivity," *IEEE Trans. Microwave Theory Tech.,* Vol. MTT-23, 199–208, 1975.
23. Verplanken, M. and J. Van Bladel, "The electric-dipole resonances of ring resonators of very High permittivity," *IEEE Trans. Microwave Theory Tech.,* Vol. MTT-24, 108–112, 1976.
24. Verplanken, M. and J. Van Bladel, "The magnetic-dipole resonances of ring resonators of very high permittivity," *IEEE Trans. Microwave Theory Tech.,* Vol. MTT-27, 328–333, 1979.
25. Kaifez, D., A. W. Glisson, and J. James, "Computed modal field distribution for isolated dielectric resonators," *IEEE Trans. Microwave Theory Tech.,* Vol. MTT-32, 1609–1616, 1984.
26. Mongia, R. K. and B. Bhat, "Accurate resonant frequencies of cylindrical dielectric resonators using a simple analytical technique," *Electron. Lett.,* Vol. 21, 479–480, 1985.
27. Zheng, W., "Computation of omplex resonance frequencies of isolated composite objects," *IEEE Trans. Microwave Theory Tech.,* Vol. MTT-37, 953–961, 1989.

28. Mongia, R. K., C. L. Larose, S. R. Mishra, and P. Bhartia, "Accurate measurement of Q-factors of isolated dielectric resonators," *IEEE Trans. Microwave Theory Tech.,* Vol. MTT-42, 1463–1466, 1994.
29. Uzunoglu, N. K., N. G. Alexopoulos, and J. G. Fikioris, "Radiation properties of microstrip dipoles," *IEEE Trans. Antennas Propagat.,* Vol. AP-27, 853–858, 1979.
30. Jones, D. S., *Theory of Electromagnetism,* Oxford: Pergamon Press, 1964.
31. Kaklamani, D. I. and N. K. Uzunoglu, "Scattering from a conductive rectangular plate covered by a thick dielectric layer and excited from a dipole or a plane wave," *IEEE Trans. Antennas Propagat.,* Vol. AP-42, 1065–1076, 1994.
32. Abramowitz, M. and I. A. Stegun, *Handbook of Mathematical Functions,* Dover Publications, Inc., New York, 1970.
33. Polychronopoulos, S., "Contribution to the development of broadband optical networks," Ph.D. Thesis, NTUA, July 1993.